RSC Advances

PAPER

View Article Online
View Journal | View Issue

Cite this: *RSC Adv.*, 2017, **7**, 53111

Electronic structure and properties of $RbTiOPO_4$:Ta crystals

Ziqing Li,[ab] Yang Chen,[a] Pengfei Zhu,[a] Nianjing Ji,[a] Xiulan Duan*[a] and Huaidong Jiang *[ab]

RTP crystals doped with four different Ta concentrations were grown by high-temperature solution method. Ta dopants changed the growth habit of RTP and the (100) faces were more developed than the other crystal faces. The chemical composition and electronic structure were analyzed using Electron Probe Microanalysis (EPMA) and X-ray photoelectron spectroscopy (XPS). Ta elements could easily incorporate into RTP crystals from the melt due to the large distribution coefficient. As Ta content increased, the Rb 3d, Ti 2p, P 2p, O 1s XPS spectra showed a shift towards higher binding energy. The relative Ta atomic concentration in RTP:Ta crystals was calculated and it was determined that the molar ratio between Ta and Ti was higher than the nominal ratio. The thermal properties and SHG efficiency were also studied. Ta dopants decreased the transition temperature from the orthorhombic RTP phase to the cubic RTP phase and increased the decomposition temperature of the cubic RTP phase. When the Ta concentration increased to 9 mol%, the specific heat of the doped crystal was 1.5 times that of pure RTP crystal at 300 °C and SHG intensity was improved by 59% when compared with pure RTP. The results show that Ta doping is helpful for improvement of SHG efficiency and increasing resistance to laser irradiation.

Received 17th September 2017
Accepted 4th November 2017

DOI: 10.1039/c7ra10310g

rsc.li/rsc-advances

Introduction

Since the last decade, $KTiOPO_4$ (KTP) family crystals have been widely used in many applications such as nonlinear optics, electro-optics (EO) and optical wave guide devices, owing to their high nonlinear optical properties, high electro-optical coefficients, high optical damage threshold, low dielectric constant, and high chemical stability.[1–5] $RbTiOPO_4$ (RTP) is an isostructural analogue to KTP which belongs to the orthorhombic crystal system, space group $Pna2_1$.[6] Compared to KTP, RTP crystals have lower conductivity, higher EO coefficient and higher damage threshold (1.8 times higher than that of KTP), which makes RTP more suitable for high-power applications.[7,33] Nowadays, RTP has been used as a commercial EO Q-switch.[8,9]

Metal ion substitution of different cation positions in RTP basic framework can actually broaden the application of RTP crystals. For example, doping with lanthanide ions can make RTP matrix achieve self-induced effects.[10–13] Self-induced effect in crystals is an interesting phenomenon, combining both nonlinear optic properties and ion photoluminescence to realize simple and integration laser devices. However, attempts to dope RTP crystals with lanthanide ions have shown too low distribution coefficients and failed to realize the effect.[14] An effective method to increase the distribution coefficients of the lanthanide ions was carried out using codopants such as Nb^{5+} and Ta^{5+}.[15]

Ta^{5+} in RTP lattice has been reported to expand the crystal structure, favoring the incorporation of more rare earth ions into the lattice.[16] Moreover, Ta^{5+} serves as charge compensation to stabilize the electroneutrality of crystals by creating vacancies, allowing a higher rare earth ion concentration to incorporate into the crystals. Furthermore, Ta^{5+} doped KTP has been reported to substantially increase the optical birefringence of KTP and to blueshift the SHG cutoff wavelengths for propagation.[17] This indicates the possibility of crystal property improvement in RTP:Ta crystals. To our knowledge, there is still little information about the electronic structure and physical characterization of RTP:Ta crystals.

In this study, RTP crystals doped with different Ta concentrations were grown by high-temperature solution method. The chemical composition was characterized through Electron Probe Microanalysis (EPMA). X-ray photoelectron spectroscopy (XPS) was used to study the electronic structure of RTP:Ta crystals. The thermal properties and nonlinear optical properties of RTP:Ta crystals and nonlinear optical applications were presented. The relationship between electronic structure and thermal stability was also discussed.

[a]*State Key Laboratory of Crystal Materials, Institute of Crystal Materials, Shandong University, Jinan 250100, P. R. China. E-mail: xlduan@sdu.edu.cn*

[b]*School of Physical Science and Technology, ShanghaiTech University, 201210, Shanghai, China. E-mail: jianghd@shanghaitech.edu.cn*

Experimental section

Crystal growth

RTP:Ta crystals were grown by spontaneous crystallization technique from a high-temperature solution system. We used Rb_2CO_3 (JiangXi Dongpeng New Materials Co., Ltd., 99.9%), $NH_4H_2PO_4$ (Sinopharm Chemical Reagent Co., Ltd., 99.5%), TiO_2 (TianJin Chemical Reagent Factory, 99.9%) and Ta_2O_5 (Aladdin Chemistry Co., Ltd., 99.9%) as raw materials. The initial reagents were mixed and heated until the decomposition gases of NH_3, H_2O and CO_2 were released. Then, the temperature was kept at the level of about 100 K above saturation temperature for 24 h to obtain homogeneous flux solution. Platinum wires were dipped into the flux solution and the temperature was decreased until a large number of small crystals were precipitated on the platinum wires. The obtained crystals were sufficient for further characterization.

Powder X-ray diffraction

In order to confirm the phase purity of RTP:Ta, we performed X-ray powder diffraction analysis through a D8 Advance diffractometer (Bruker AXS, Advanced X-ray Solutions) equipped with Cu-K radiation (λ = 0.15406 nm) and a graphite monochromator in the 2θ range of 15.0–65.0°. The crystal structure was identified by Version 6 Analysis software according to the peak values of 2θ in the standard pattern.

EPMA

Electron Probe Microanalysis (Shimadzu, EPMA-1720H) was used to measure the doping concentrations in the RTP:Ta crystals with the parameters of AccV = 15 kV, BC = 10 nA and size = MIN. Error in composition analysis was ±1%.

X-ray photoelectron spectra

To obtain the electronic structure of the RTP:Ta, X-ray photoelectron spectra (XPS) were recorded using a Thermo Fisher ESCALAB 250 X-ray photoelectron spectrometer with monochromatic Al Kα X-ray radiation. The background pressure in the analysis chamber at room temperature was in the range of 10^{-9} to 10^{-10} Pa. The measurement was carried out in constant analyzer energy (CAE) scan mode. Initial survey scans were performed at pass energy of 150 eV, dwell time of 50 ms and energy step size of 1 eV. Narrow scans of C 1s, Rb 3d, Ti 2p, P 2p, O 1s regions were acquired at pass energy of 20 eV, dwell time of 50 ms and energy step size of 0.05 eV. The binding energy of samples was calibrated using C 1s peak (284.6 eV) as a reference. The spectra were successfully deconvoluted using a Gaussian–Lorentzian curve fitting program after background subtraction. The error of binding energy is ±0.1 eV.

TG/DTA

TG/DTA was carried out using a Diamond TG/DTA analyzer (Perkin Elmer, Inc.). The samples were heated at a rate of 5 °C min^{-1} from room temperature to 1230 °C. Specific heat was measured using a Diamond differential scanning calorimeter over the temperature range of 20–300 °C in air atmosphere.

SHG

Powder second harmonic generation measurements were performed using the Kurtz and Perry powder method.[18] The RTP:Ta crystals were ground into powders and sieved into particles with size of 21–38 μm. The samples were loaded in a 1 mm-thick quartz holder and irradiated with a pulsed Nd:YAG laser at a wavelength of 1064 nm. Pure RTP was used as a reference.

Results and discussion

Spontaneous nucleation crystal growth and chemical composition

RTP:Ta crystals were obtained by spontaneous crystallization technique. For growing RTP crystals with different Ta concentrations, we fixed the Rb_2O/P_2O_5 ratio and then substituted part of the Ti element with Ta element in the melt. The Ta concentration $\left(\frac{[Ta]}{[Ti]+[Ta]}\right)$ was from 3 mol% up to 9 mol% in melt. The Ta doping concentration in the crystals was obtained through Electron Probe Microanalysis (EPMA). The distribution coefficients of Ta were calculated according to the following expression:

$$K_{Ta} = \frac{\left(\frac{[Ta]}{[Ti]+[Ta]}\right)_{crystal}}{\left(\frac{[Ta]}{[Ti]+[Ta]}\right)_{melt}}$$

Table 1 summarizes the obtained results. Rb_6 is the abbreviation of the $Rb_6P_4O_{13}$ solvent in the melt. The distribution coefficient K_{Ta} is usually larger than unity. This indicates that Ta elements can easily incorporate into RTP crystals from the melt. However, K_{Ta} value decreased when Ta concentration in the melt increased to 9 mol%. This trend has also been observed in KTP:Ta crystals.[19] Ta^{5+} ions are expected to replace Ti^{4+} ions in the structure and stabilize the electroneutrality of the crystals by creating Rb^+ vacancies.[24]

X-ray powder diffraction analysis

The results of X-ray powder diffraction are shown in Fig. 1. The XRD patterns were collected in the scan range of 15–65° with

Table 1 Chemical compositions and distribution coefficients of Ta in RTP:Ta crystal[a]

A	B	C	D	E
44.21–33.07–22.03–0.34	0.576	3	3.22 ± 0.01	1.06
44.21–33.07–21.58–0.56	0.560	5	5.40 ± 0.01	1.08
44.21–33.07–21.13–0.79	0.544	7	7.74 ± 0.01	1.10
44.21–33.07–20.67–1.02	0.529	9	7.81 ± 0.01	0.87

[a] (A) solution composition (Rb_2O–P_2O_5–TiO_2–Ta_2O_5) (mol%). (B) RTP/Rb_6 (mass ratio). (C) Ta concentration in melt (mol%). (D) Ta concentration in crystal (mol%). (E) distribution coefficient of Ta (K_{Ta}).

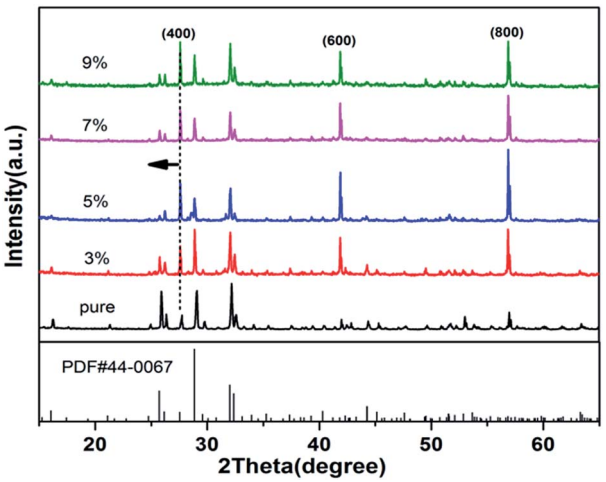

Fig. 1 XRD patterns of pure and Ta-doped RTP crystals.

a step of 0.02°. The XRD patterns of RTP:Ta crystals are well indexed with that of pure RTP (PDF#44-0067). This indicates that the Ta^{5+} ions do not change the RTP phase to a certain extent and all the doped RTP crystals are highly crystallized. The peak positions show an evident shift (short dash and black arrow) towards lower diffraction angle in RTP:Ta crystals, which indicates that the lattice constants become larger. The larger lattice constants could result from the larger atomic radius of Ta^{5+} (0.640 Å) compared to Ti^{4+} (0.605 Å). It is interesting to find that the diffraction peak intensity of (100) faces become clearly stronger in RTP:Ta crystals. The result indicates that the (100) face is well developed for RTP:Ta crystals, which can be confirmed by SEM graphs (shown in Fig. 2). This phenomenon in XRD has not been reported before although the morphology change in doped RTP crystals has been known.[20] However, currently, there is little explanation and an effort to identify the possible reasons is being made.

Electronic structure

The survey X-ray photoelectron spectra of RTP:Ta crystals are depicted in Fig. 3. The photoemission and Auger lines of the constituent elements were detected. The C 1s core-level peak at 284.6 eV was determined to be a hydrocarbon contamination. Ca was also detected as surface contamination only in pure RTP crystal.

The high-resolution XPS spectra of Rb 3d were recorded (Fig. 4(a)). The Rb 3d level consists of $3d_{5/2}$ and $3d_{3/2}$ components with intensity ratio of 3 : 2 due to spin orbit coupling. The distance between the doublet peaks is 1.4 eV, which is close to the value previously reported.[21] The peak of Rb $3d_{5/2}$ for the pure RTP crystal is 108.9 eV, which is in good agreement with the data reported by Atuchin *et al.*[22] Compared to that in pure RTP, the Rb 3d level in RTP:Ta crystals shows a 0.3 eV shift towards higher binding energy. The binding energy shift reaches 0.4 eV when doping concentration comes to 9 mol%. The higher binding energy of Rb 3d in RTP:Ta crystal primarily results from the electronic structure change of Rb–O bonds when dopants

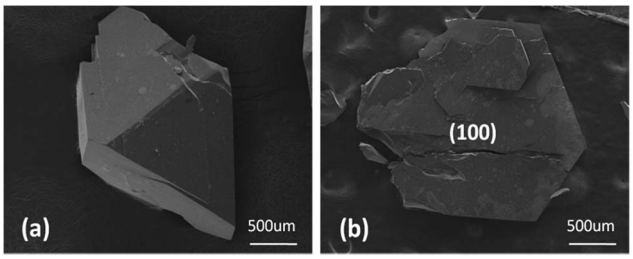

Fig. 2 The SEM observation of the morphology of (a) pure RTP and (b) RTP:Ta crystals. The (100) face was more developed after doping Ta ions.

enter into the RTP lattice. This could be explained by the Pauling electronegativity concept.[23] The Ta^{5+} ions have more active electronegativity and more easily attract electrons than Rb^{+} ions. This largely influences the electrons migrating from Rb^{+} to Ta^{5+}. Because the valence electron density of Rb^{+} is shifted towards Ta^{5+}, it will be difficult to eject an electron from Rb^{+} ion; as a result, the Rb 3d binding energy increases.

The detailed spectra of the Ti 2p doublet are shown in Fig. 4(b). Due to spin orbit coupling, Ti $2p_{3/2}$ and Ti $2p_{1/2}$ are separated by 5.8 eV with intensity ratio of 2 : 1. This data is similar to 5.76 eV for TiO_2 as previously reported in literature.[21] For a pure RTP crystal, the binding energy values are 458.7 eV for Ti $2p_{3/2}$ and 464.5 eV for Ti $2p_{1/2}$, respectively.

The binding energies of the Ti 2p doublet peaks show a shift to higher binding energy with increase in Ta^{5+} in RTP:Ta crystals. Such a phenomenon could be associated with the replacement of Ti by Ta element.[24]

The high-resolution XPS spectra of P 2p peak are shown in Fig. 5(a). These obtained values resemble previously reported data for RTP crystal.[22] The binding energy of P 2p is from 132.8 eV to 133.2 eV. There is a 0.4 eV shift to higher binding energy as the doping concentration increases from 0 to 9 mol%.

Fig. 5(b) shows the high-resolution XPS spectra of O 1s levels in pure and RTP:Ta crystals. As shown in Fig. 5(b), the binding

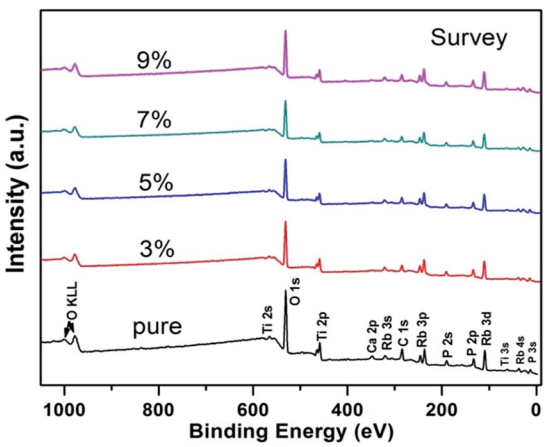

Fig. 3 Survey X-ray photoelectron spectra of pure and RTP:Ta crystals. The different elements associated with electronic state are denoted for respective peaks.

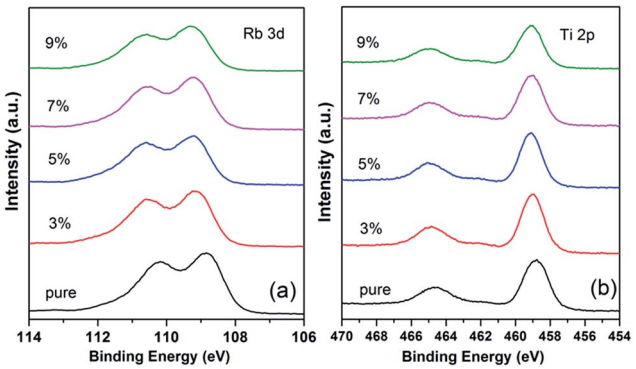

Fig. 4 High-resolution X-ray photoelectron spectra of (a) Rb 3d core level and (b) Ti 2p core level of pure and RTP:Ta crystals.

energy of the O 1s in pure RTP is 530.8 eV, which is close to the literature value (530.4 eV) in pure RTP.[22] The O 1s spectra are asymmetric and can be deconvoluted into two peaks. The peaks at low and high binding energy are respectively assigned to lattice oxygen and absorbed oxygen.[25,26] There is an evident chemical shift in O 1s towards higher binding energy as the Ta concentration increases in RTP crystal. The binding energy shift of O 1s reaches 0.4 eV at 3 mol% Ta doping concentration. There is a 0.5 eV shift to higher binding energy when the Ta doping concentration increases to 9 mol%. The binding energies for Rb $3d_{5/2}$, Ti 2p, P 2p, and O 1s core levels of pure and RTP:Ta crystals are collected in Table 2.

The photoelectron spectra of Ta 4f are displayed in Fig. 6. We observed Ca 3p core level only in pure RTP crystal, which could be due to surface contamination. It is clear that Ta ions were introduced successfully into the RTP lattice. The high-resolution XPS spectra of Ta 4f are slightly complicated because of the superposition of Ta 4f peak, O 2s peak and Rb 4s peak in RTP:Ta crystals. The peaks at around 23.4 eV and 29.1 eV are assigned to O 2s and Rb 4s respectively. In RTP:Ta crystals, Ta $4f_{7/2}$ and Ta $4f_{5/2}$ peaks appeared at 26.3 eV and 28.2 eV respectively. The spin–orbit doublet separation is 1.9 eV, which corresponds to the data reported in literature.[27,28] The intensity ratio between Ta $4f_{7/2}$ and Ta $4f_{5/2}$ peaks is 4 : 3. The detailed binding energies for Ta $4f_{7/2}$, Rb 4s, Ca 3p, and O 2s

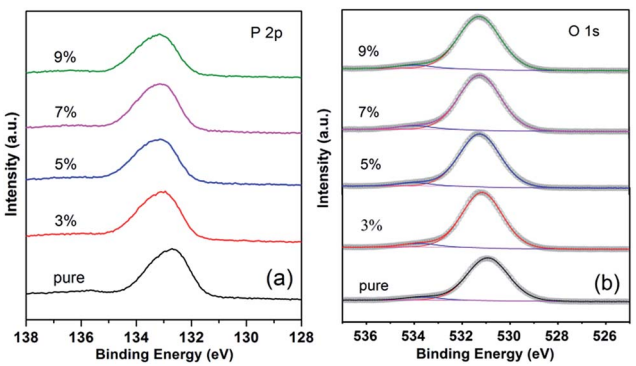

Fig. 5 High-resolution X-ray photoelectron spectra of (a) P 2p core level and (b) O 1s core level of pure and RTP:Ta crystals.

Table 2 Binding energy values for Rb $3d_{5/2}$, Ti $2p_{3/2}$, P 2p, O 1s core levels of pure and Ta-doped RTP crystals

Composition (mol%)	Rb $3d_{5/2}$ (±0.1 eV)	Ti $2p_{3/2}$ (±0.1 eV)	P 2p (±0.1 eV)	O 1s (±0.1 eV)
Pure	108.9	458.7	132.8	530.8
3%	109.2	459.0	133.0	531.2
5%	109.2	459.1	133.1	531.2
7%	109.2	459.1	133.1	531.2
9%	109.3	459.1	133.2	531.3

core levels of RTP:Ta crystals are listed in Table 3. The relative atomic concentration between Ta and Ti in RTP:Ta crystals is calculated using Avantage software. The data are recorded in Table 4 with error of approximately 5%. The obtained results suggest that the molar ratio between Ta and Ti actually increases compared with the nominal ratio.

Thermal properties

Fig. 7(a) shows the results of DTA analysis of pure and RTP:Ta crystals. We identify two clear endothermic peaks for each curve. One is assigned to the transition temperature (dash line) from the orthorhombic RTP phase to the cubic RTP phase; the other is assigned to the decomposition temperature (arrows) of the cubic RTP phase.[29,30] As shown in this figure, with Ta concentration increasing in the RTP:Ta crystals, the transition temperature from the orthorhombic RTP phase to the cubic RTP phase decreases and the decomposition temperature of cubic RTP phase increases. The decrease in decomposition temperature (arrows) with respect to Ta concentration in RTP:Ta crystals can also be verified by TG analysis in Fig. 7(b). This change has been observed in RTP:Nb crystals and could be explained by the stability of the cubic RTP phase after doping with Ta^{5+}, in which lower activation energy is needed to generate the new cubic phase from the orthorhombic phase.[31]

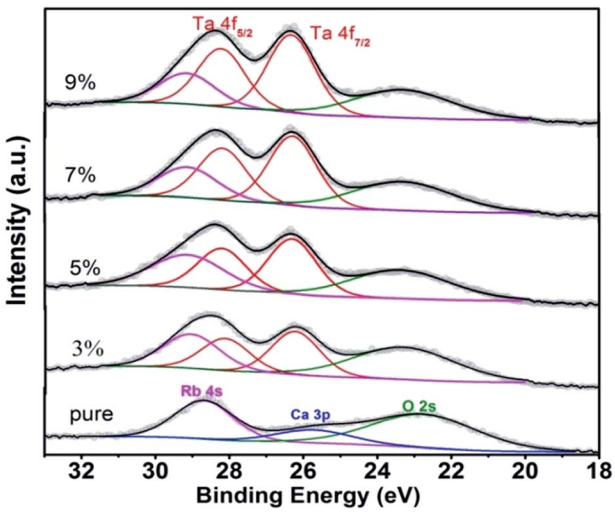

Fig. 6 High-resolution X-ray photoelectron spectra of Ta 4f core level of pure and RTP:Ta crystals.

Table 3 Binding energy values for Ta $4f_{7/2}$, Rb 4s, Ca 3p, O 2s core levels of pure and Ta-doped RTP crystals

Composition (mol%)	Ta $4f_{7/2}$ (±0.1 eV)	Rb 4s (±0.1 eV)	Ca 3p (±0.1 eV)	O 2s (±0.1 eV)
Pure	—	28.7	25.7	22.9
3%	26.2	29.1	—	23.3
5%	26.3	29.1	—	23.3
7%	26.3	29.1	—	23.4
9%	26.3	29.1	—	23.4

Because the cubic phase is more stable, more energy is required to decompose it. This leads to the increase in decomposition temperature.

For laser and nonlinear crystals, specific heat is an important factor influencing laser damage threshold.[32] Higher specific heat for crystals is beneficial to sustain against higher laser irradiation. The specific heat curves of pure and Ta doped RTP crystals as a function of temperature are shown in Fig. 8. As shown in Fig. 8, the specific heat increases with increase in temperature for all the crystals. There is an evident augment in specific heat as the Ta concentration increases particularly in the high temperature range. When the Ta doping concentration increases to 9 mol%, the specific heat of the doped crystal reaches 1.34 J g^{-1} K^{-1} at 300 °C, which is 1.5 times as much as that of pure RTP crystal. This indicates that RTP:Ta crystal is more stable for enduring irradiation and has high laser damage threshold, making the crystal suitable for laser and nonlinear optical applications.

The variation of binding energy introduced by Ta in RTP crystal is the result of changing electronic structure. The higher binding energy of Rb^+ indicates less valence electron density of Rb^+, thus Rb^+ easily loses electrons. We assume that more positive charge transfers to Rb^+ while more negative charge transfers to anionic groups such as $[TiO_6]^{8-}$ and $[PO_4]^{3-}$ after doping with Ta in RTP. This causes stronger electro-static attraction between Rb^+ and anionic groups.[36–38] This could explain the enhancement of thermal stability in RTP:Ta crystals.

Table 4 Relative atomic concentration for Ta and Ti estimated from XPS data

Composition (mol%)	Ta 4f atomic%	Ti 2p atomic%
3%	5.7	94.3
5%	8.4	91.6
7%	10.8	89.2
9%	12.3	87.7

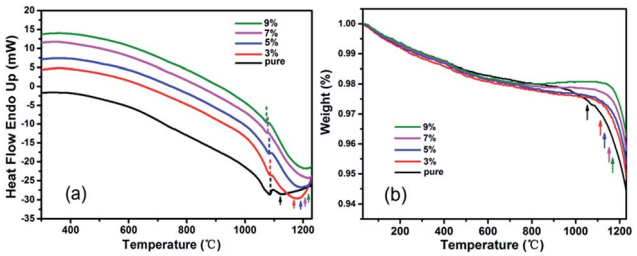

Fig. 7 The DTA (a) and TG (b) for pure and RTP:Ta crystals.

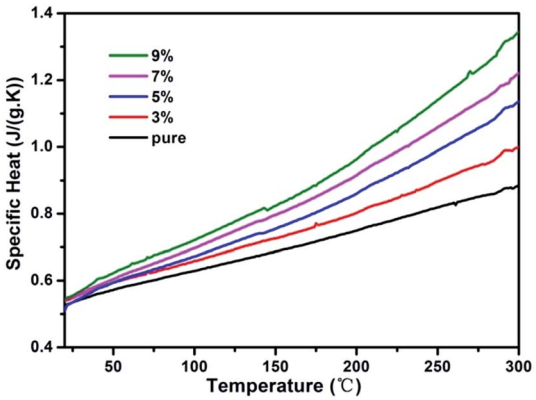

Fig. 8 Specific heat curves of pure and RTP:Ta crystals as a function of temperature.

Table 5 Second-harmonic generation intensity of RTP:Ta crystals in relation to pure RTP crystal

Doping concentration	$(SHG\ intensity)_{RTP:Ta}/(SHG\ intensity)_{RTP}$
3%	1.14
5%	1.32
7%	1.45
9%	1.59

SHG

The second-harmonic generation intensity values of RTP:Ta crystals in relation to pure RTP crystal are listed in Table 5. The nonlinear optical parameters of pure RTP are well-established in the literature,[34] and therefore the doping results are referred to those of pure RTP. As Ta doping concentration increases, the SHG intensity of RTP:Ta crystal increases. When the Ta concentration reaches 9 mol%, the SHG intensity is improved by 59% compared to pure RTP. This means Ta^{5+} doping is beneficial to improve SHG intensity of RTP crystals. This enhancement could be due to the larger atomic radius of Ta^{5+} (0.640 Å) compared to Ti^{4+} (0.605 Å). The substitution of Ta^{5+} for Ti^{4+} in RTP increases the degree of distortion of the TiO_6 octahedron,[35] which enhances SHG intensity in RTP:Ta crystals. Ta doping RTP crystals for improvement of SHG efficiency makes them better for laser and nonlinear optical applications.

Conclusions

RTP:Ta crystals were successfully grown by spontaneous crystallization technique. The Ta dopants changed the growth habit of RTP, and the (100) faces were more developed than the other crystal faces. Ta elements could easily incorporate into RTP crystals from melt due to the large distribution coefficient. As

the Ta content increases, the Rb 3d, Ti 2p, and P 2p XPS spectra show a 0.2–0.4 eV shift towards higher binding energy, while O 1s XPS spectra show a 0.4–0.5 eV shift towards higher binding energy. The relative Ta atomic concentration was calculated and showed that the molar ratio between Ta and Ti was higher than the nominal ratio. Ta dopants increase the decomposition temperature of cubic RTP phase. The specific heat is significantly enhanced in RTP:Ta crystals and increases with increasing Ta content. The SHG intensity also increases with the increase in Ta content. For the crystal doped with 9 mol% Ta, the specific heat of the doped crystal was 1.5 times as much as that of pure RTP crystal at 300 °C, and the SHG intensity was improved by 59% compared to pure RTP. The relationship between the thermal and SHG properties and the crystal structure has been discussed. Ta doped RTP crystals can be widely used in laser and nonlinear optical applications.

Conflicts of interest

There are no conflicts to declare.

Acknowledgements

This work was supported by the Major State Basic Research Development Program of China (No. 2014CB910401) and the National Natural Science Foundation of China (51672160 and 31430031).

Notes and references

1 N. Sorokina and V. Voronkova, *Crystallogr. Rep.*, 2007, **52**, 80–93.
2 Y. Zhang, Y. Leng, J. Liu, N. Ji, X. Duan, J. Li, X. Zhao, J. Wang and H. Jiang, *CrystEngComm*, 2015, **17**, 3793–3799.
3 J. Bierlein and C. Arweiler, *Appl. Phys. Lett.*, 1986, **49**, 917–919.
4 Y. Zhang, H. Wang, C. Ma, Y. Jia, J. Li, J. Wang, R. Boughton and H. Jiang, *J. Cryst. Growth*, 2015, **412**, 67–71.
5 J. D. Bierlein, A. Ferretti, L. H. Brixner and W. Y. Hsu, *Appl. Phys. Lett.*, 1987, **50**, 1216–1218.
6 P. Thomas, S. Mayo and B. Watts, *Acta Crystallogr., Sect. B: Struct. Sci.*, 1992, **48**, 401–407.
7 V. Y. Shur, E. Pelegova, A. Akhmatkhanov and I. Baturin, *Ferroelectrics*, 2016, **496**, 49–69.
8 J. Wang, H. Yu, Y. Wu and R. Boughton, *Engineering*, 2015, **1**, 192–210.
9 Y. S. Oseledchik, A. Pisarevsky, A. Prosvirnin, V. Starshenko and N. Svitanko, *Opt. Mater.*, 1994, **3**, 237–242.
10 J. Carvajal, V. Nikolov, R. Solé, J. Gavaldà, J. Massons, M. Rico, C. Zaldo, M. Aguiló and F. Díaz, *Chem. Mater.*, 2000, **12**, 3171–3180.
11 J. Carvajal, R. Sole, J. Gavalda, J. Massons, M. Rico, C. Zaldo, M. Aguiló and F. Díaz, *J. Alloys Compd.*, 2001, **323**, 231–235.
12 J. Carvajal, R. Solé, J. Gavaldà, J. Massons, M. Aguiló and F. Díaz, *Cryst. Growth Des.*, 2001, **1**, 479–484.
13 J. Carvajal, R. Solé, J. Gavaldà, J. Massons and M. Aguiló, *Opt. Mater.*, 2003, **24**, 425–430.
14 M. Rico, C. Zaldo, J. Massons and F. Díaz, *J. Phys.: Condens. Matter*, 1998, **10**, 10101.
15 A. Peña, J. J. Carvajal, M. C. Pujol, X. Mateos, M. Aguiló, F. Díaz, V. Petrov, P. Segonds and B. Boulanger, *Opt. Express*, 2007, **15**, 14580–14590.
16 A. Peña, J. Carvajal, J. Massons, J. Gavaldà, F. Díaz and M. Aguiló, *Chem. Mater.*, 2007, **19**, 4069–4076.
17 L. Cheng, L. Cheng, R. Harlow and J. Bierlein, *Appl. Phys. Lett.*, 1994, **64**, 155–157.
18 S. Kurtz and T. Perry, *J. Appl. Phys.*, 1968, **39**, 3798–3813.
19 V. Voronkova, V. Yanovskii, T. Y. Losevskaya, S. Y. Stefanovich, S. Zver'kov, O. Alekseeva and N. Sorokina, *Crystallogr. Rep.*, 2004, **49**, 123–129.
20 J. Carvajal, C. Woensdregt, R. Solé, F. Díaz and M. Aguiló, *Cryst. Growth Des.*, 2006, **6**, 2667–2673.
21 C. D. Wagner, *Handbook of x-ray photoelectron spectroscopy: a reference book of standard data for use in x-ray photoelectron spectroscopy*, Physical Electronics Division, Perkin-Elmer Corp., 1979.
22 V. Atuchin, V. Kesler, G. Meng and Z. Lin, *J. Phys.: Condens. Matter*, 2012, **24**, 405503.
23 L. Pauling, *The nature of the chemical bond and the structure of molecules and crystals: an introduction to modern structural chemistry*, Cornell university press, 1960.
24 J. Carvajal, J. García-Muñoz, R. Solé, J. Gavaldà, J. Massons, X. Solans, F. Díaz and M. Aguiló, *Chem. Mater.*, 2003, **15**, 2338–2345.
25 V. Kumar, H. Swart, O. Ntwaeaborwa, R. Kroon, J. Terblans, S. Shaat, A. Yousif and M. Duvenhage, *Mater. Lett.*, 2013, **101**, 57–60.
26 K. Tabata, T. Choso and Y. Nagasawa, *Surf. Sci.*, 1998, **408**, 137–145.
27 R. Nyholm, A. Berndtsson and N. Martensson, *J. Phys. C: Solid State Phys.*, 1980, **13**, L1091.
28 D. M. Riffe and G. Wertheim, *Phys. Rev. B*, 1993, **47**, 6672.
29 L. Cheng, E. McCarron, J. Calabrese, J. Bierlein and A. Ballman, *J. Cryst. Growth*, 1993, **132**, 280–288.
30 G. Marnier, B. Boulanger and B. Menaert, *J. Phys.: Condens. Matter*, 1989, **1**, 5509.
31 J. Carvajal, R. Sole, J. Gavaldà, J. Massons, F. Diaz and M. Aguilo, *Chem. Mater.*, 2003, **15**, 2730–2736.
32 B. Teng, J. Wang, Z. Wang, X. Hu, H. Jiang, H. Liu, X. Cheng, S. Dong, Y. Liu and Z. Shao, *J. Cryst. Growth*, 2001, **233**, 282–286.
33 F. Laudenbach, B. Jin, C. Greganti, M. Hentschel, P. Walther and H. Hübel, *Phys. Rev. Appl.*, 2017, **8**, 024035.
34 Y. Oseledchik, A. Pisarevsky, A. Prosvirnin, V. Starshenko and N. Svitanko, *Opt. Mater.*, 1994, **3**, 237–242.
35 K. Zhang and X. Wang, *Chin. Sci. Bull.*, 2001, **46**, 2028–2036.
36 M. Upton, C. Wei, M. Chou, T. Miller and T. Chiang, *Phys. Rev. Lett.*, 2004, **93**, 026802.
37 A. Riefer, M. Friedrich, S. Sanna, U. Gerstmann, A. Schindlmayr and W. Schmidt, *Phys. Rev. B*, 2016, **93**, 075205.
38 J. Wen, Y. Yeung, L. Ning, C. Duan, Y. Huang, J. Zhang and M. Yin, *J. Alloys Compd.*, 2017, **713**, 28–37.

